NANO LETTERS

Subscriber access provided by KUNGL TEKNISKA HOGSKOLAN

Communication

Integration of colloidal PbS/CdS quantum dots with plasmonic antennas and superconducting detectors on a silicon nitride photonic platform

Lukas Elsinger, Ronan Gourgues, Iman Esmaeil Zadeh, Jorick Maes, Antonio Guardiani, Gabriele Bulgarini, Silvania F. Pereira, Sander N. Dorenbos, Valery Zwiller, Zeger Hens, and Dries Van Thourhout

Nano Lett., **Just Accepted Manuscript** • DOI: 10.1021/acs.nanolett.9b01948 • Publication Date (Web): 17 Jul 2019

Downloaded from pubs.acs.org on July 18, 2019

Just Accepted

"Just Accepted" manuscripts have been peer-reviewed and accepted for publication. They are posted online prior to technical editing, formatting for publication and author proofing. The American Chemical Society provides "Just Accepted" as a service to the research community to expedite the dissemination of scientific material as soon as possible after acceptance. "Just Accepted" manuscripts appear in full in PDF format accompanied by an HTML abstract. "Just Accepted" manuscripts have been fully peer reviewed, but should not be considered the official version of record. They are citable by the Digital Object Identifier (DOI®). "Just Accepted" is an optional service offered to authors. Therefore, the "Just Accepted" Web site may not include all articles that will be published in the journal. After a manuscript is technically edited and formatted, it will be removed from the "Just Accepted" Web site and published as an ASAP article. Note that technical editing may introduce minor changes to the manuscript text and/or graphics which could affect content, and all legal disclaimers and ethical guidelines that apply to the journal pertain. ACS cannot be held responsible for errors or consequences arising from the use of information contained in these "Just Accepted" manuscripts.

is published by the American Chemical Society. 1155 Sixteenth Street N.W., Washington, DC 20036

Published by American Chemical Society. Copyright © American Chemical Society. However, no copyright claim is made to original U.S. Government works, or works produced by employees of any Commonwealth realm Crown government in the course of their duties.

Integration of colloidal PbS/CdS quantum dots with plasmonic antennas and superconducting detectors on a silicon nitride photonic platform

Lukas Elsinger,[†,‡,#] Ronan Gourgues,[¶,#] Iman E. Zadeh,[§] Jorick Maes,[‖,‡] Antonio Guardiani,[¶] Gabriele Bulgarini,[¶] Silvania F. Pereira,[§] Sander N. Dorenbos,[¶] Val Zwiller,[⊥] Zeger Hens,[‖,‡] and Dries Van Thourhout*[,†,‡]

†*Photonics Research Group, Ghent University - imec, 9052 Ghent, Belgium*

‡*NB-photonics, Ghent University, 9052 Ghent, Belgium*

¶*Single Quantum B.V., 2628 CJ Delft, The Netherlands*

§*Optics Research Group, Delft University of Technology, 2628 CJ Delft, The Netherlands*

‖*Physics and Chemistry of Nanostructures Group, Ghent University, 9000 Ghent, Belgium*

⊥*Department of Applied Physics, KTH, Stockholm 106 91, Sweden*

#*equal contribution*

E-mail: dries.vanthourhout@ugent.be

Abstract

Single-photon sources and detectors are indispensable building blocks for integrated quantum photonics, a research field that is seeing ever increasing interest for numerous applications. In this work we implemented essential components for a Quantum Key Distribution (QKD) transceiver on a single photonic chip. Plasmonic antennas

on top of silicon nitride waveguides provide Purcell enhancement with a concurrent increase of the count rate, speeding up the microsecond radiative lifetime of IR-emitting colloidal PbS/CdS Quantum Dots (QDs). The use of low-fluorescence silicon nitride with a waveguide loss smaller than 1 dB/cm, made it possible to implement high extinction ratio optical filters and low insertion loss spectrometers. Waveguide-coupled Superconducting Nanowire Single-Photon Detectors (SNSPDs) allow for low time-jitter single-photon detection. To showcase the performance of the components, we demonstrate on-chip lifetime spectroscopy of PbS/CdS QDs. The method developed in this paper is predicted to scale down to single QDs and newly developed emitters can be readily integrated on the chip-based platform.

Keywords

colloidal quantum dots, plasmonic antennas, superconducting nanowire single photon detector, hybrid integrated photonics

Main

Most applications of single-photon sources in quantum optical technology have very stringent requirements on single-photon properties such as purity and indistinguishability.[1] Therefore, for a long time the most commonly used single-photon sources were based on spontaneous parametric down-conversion, which offers pure and indistinguishable heralded single-photon emission, but is probabilistic in nature.[2] Recently, epitaxial QDs have reached a high maturity level as deterministic single-photon emitters[3] enabling applications in several quantum photonic technologies.[4–6]

The unrivaled performance of SNSPDs in terms of system detection efficiency, dark count rate and temporal resolution[7–9] has made them indispensable for many quantum optics experiments. In addition, SNSPDs can be integrated with different photonic platforms while

maintaining a small footprint.[10–13] Progress has been made in integrating epitaxial QDs with SNSPDs on the same chip,[14] but the rather large waveguide loss is a main hindrance to the development of more complex photonic circuits. Hybrid integration approaches with epitaxial QDs[15–19] make use of the low waveguide loss of silicon photonics to be compliant with the requirements of quantum optics protocols.

Among other promising single photon emitters,[1] colloidal QDs are especially interesting due to recent improvements of their single-photon emission purity and stability,[20–22] while solution processing allows for a flexible integration.[23] By looking at the current performance metrics, only the application with the lowest requirements on single-photon purity and indistinguishably, Quantum Key Distribution (QKD)[1] seems to be within reach. The original BB84 QKD protocol requires single-photon sources in its security proof.[24] However, modern decoy state protocols are also provably secure using attenuated lasers as sources, although at the cost of reduced key generation rate.[25–27] QD single-photon emitters reaching the maximum average photon number per pulse of $\langle n \rangle = 1$ may outperform laser sources and have been employed for long-range QKD.[28] A chip-level implementation of QKD has been achieved with integrated lasers,[29] but remains elusive for true single-photon emitters. Key properties to be competitive with state-of-the-art decoy state protocols[27] are a fast source in the GHz range at a telecom wavelength where optical fiber losses are minimal and a narrow emission linewidth to enable Wavelength Division Multiplexing (WDM) and thus further enhance the key generation rate. Also, low-loss photonic waveguides, filters and spectrometers that retain a high average photon number $\langle n \rangle$ during the encoding and highly efficient single-photon detectors for telecom wavelengths are essential, as well as a low detector dark count rate to minimize the QKD error rate.

In this work we present a silicon nitride photonic platform that implements several of those components, as shown in Figure 1. A single chip contains colloidal QD emitters placed in the gap of plasmonic antennas that were fabricated on top of silicon nitride waveguides (I), sidewall corrugated grating filters for pump rejection (II) and a Planar Concave Grat-

ing (PCG) spectrometer (III) of which four channels are connected to waveguide-coupled SNSPDs (IV). All components were connected by low-loss photonic waveguides surrounded by metal strips to suppress stray light coupling (V).

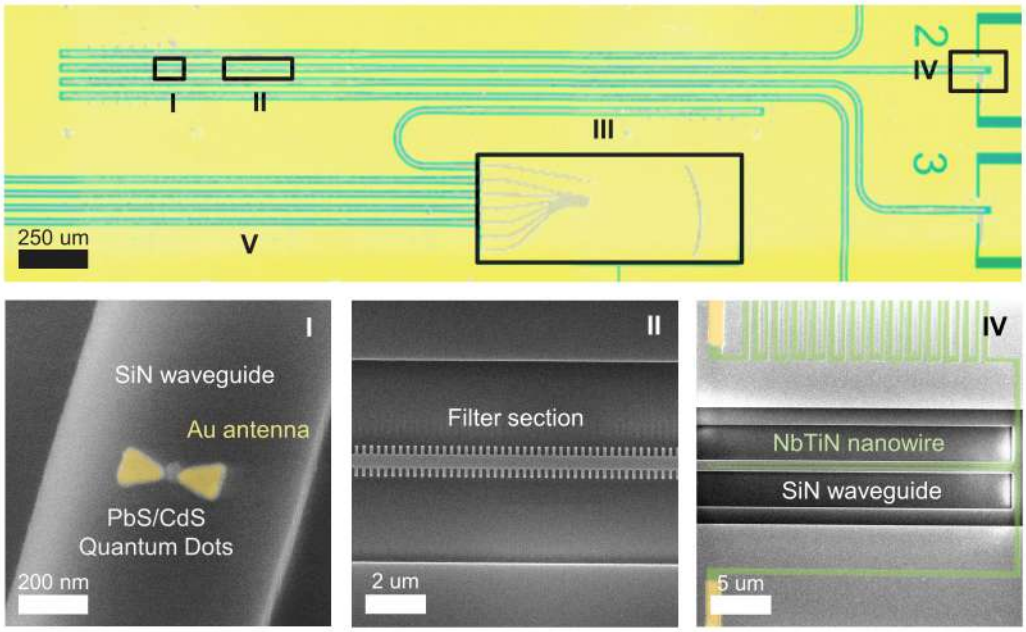

Figure 1: The silicon nitride photonic chip in consists of areas with colloidal QD emitters and plasmonic antennas (I), filters for pump rejection (II), a Planar Concave Grating (PCG) spectrometer (III) of which four channels are connected to waveguide-coupled SNSPD detectors (III). All components are connected by waveguides which are surrounded by metal strips to suppress stray light coupling (V). The false-color SEM picture (I) shows a SiN waveguide with a plasmonic bowtie antenna and a patch of colloidal QDs patterned on top of it. To suppress the 700 nm pump laser, sidewall corrugated waveguide gratings (II) were implemented. The QD emission was detected by U-shaped superconducting detectors placed underneath the SiN waveguides (IV). For measurements with SNSPDs the chip was cooled down in a helium bath cryostat to a temperature of 4.2 K.

Purcell enhancement with plasmonic antennas

For QKD fast sources are required, therefore a short radiative lifetime of QD emitters is crucial to be competitive compared to state-of-the-art implementations with attenuated pulsed lasers. Purcell enhancement of emitters placed in dielectric cavities or in the high local density of states (LDOS) field of plasmonic antennas is a common way to reduce the radiative lifetime without the need for engineering the emitter itself.[30–33] Here, we used the widely

studied plasmonic gap antenna in a bowtie shape[34] (30 nm evaporated gold and a gap width of 25 nm) to improve the microsecond radiative lifetime of IR-emitting colloidal PbS/CdS QDs, coupling the emission directly to silicon nitride waveguides and measuring the photoluminescence (PL) decay trace with SNSPDs located on the same chip. For reference measurements we also fabricated isolated pillars of QDs on the same waveguides.

The effect of a plasmonic antenna on an emitter is most conveniently expressed in terms of LDOS and commonly referred to as Purcell enhancement. Due to the metal losses of the antenna there is a nonradiative contribution in addition to the radiative local density of states (LRDOS), leading to a nonradiative and radiative part of the PL decay rate[32]

$$\gamma_{ant} = \gamma_{0,nr} + \gamma_{0,r}\,(\mathrm{LDOS} - \mathrm{LRDOS}) + \gamma_{0,r}\mathrm{LRDOS}, \tag{1}$$

where $\gamma_{0,nr}$ and $\gamma_{0,r}$ are the nonradiative and radiative decay rate of the emitter in absence of the antenna. We therefore first simulated the decay rate of a classical dipole emitter with a displacement vector $\mathbf{d}$ in the direction of the antenna axis using a commercial Finite Difference Time Domain (FDTD) solver (Lumerical) and extracted LDOS and LRDOS, normalizing the values to a homogeneous background medium in the absence of the antenna. For the LRDOS map in Figure 2a, the in-plane position of the dipole emitter was swept and the values were recorded for the center wavelength of the PbS/CdS QD emission at $\lambda = 1150$ nm. The false-color SEM picture of a fabricated structure in Figure 2b shows a small pillar of QDs deterministically positioned in the gap of the antenna. The simulated LDOS(λ) for a dipole emitter in the center of the gap in Figure 2d shows a broad antenna resonance that matches the PbS/CdS QD photoluminescence emission spectrum in Figure 2c. The fraction of LRDOS(λ)/LDOS(λ) gives an antenna efficiency $>70\%$ for most of the QD emission spectrum and the respective map for the center wavelength can be found in the Supporting Information Figure S6a. Figure 2d also shows a reduction and red-shift of the LRDOS(λ), when including the pillar of QDs in the simulation with refractive index data

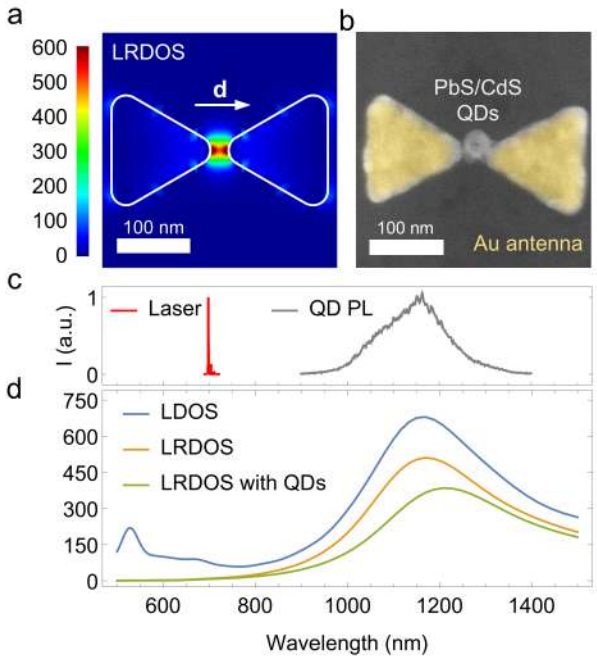

Figure 2: The map of the LRDOS in (a) results from Finite Difference Time Domain (FDTD) simulation of a dipole emitter with displacement vector **d**. The SEM micrograph of the fabricated bowtie antenna with a small patch of PbS/CdS QDs deterministically positioned in the antenna gap (b) was colored to highlight the different materials. (c) Spectrum of the excitation laser and the QD PL emission at 4.2 K. (d) Comparison of the simulated LDOS for an emitter in the center of the antenna gap and the LRDOS for an empty antenna as well as for an antenna with a QD pillar placed in the gap.

from ellipsometry measurements. Taking this into account and sweeping the position of the dipole emitter within the volume of the QD pillar, gave an average LRDOS of 150. A slight misalignment of the QD pillar 20 nm off the antenna center perpendicular to the dipole moment, as can be observed in Figure 2b reduces this value to 100, for a larger misalignment of 50 nm the enhancement factor drops to 6. The antenna also has a small resonance at the pump laser wavelength of 700 nm, which can be seen from the polarization dependent excitation enhancement maps displayed in the Supporting Information Figure S6. We confirmed the validity of the FDTD simulations by matching simulated and measured transmission spectra of an array of antennas on a glass sample (see Supporting Information Figure S5). Fabrication details and specifics of the simulation methodology can be found in

the Supporting Information S1 and S4.

The on-chip measurements were performed in a liquid helium bath cryostat (4.2 K base temperature) and we used a 700 nm diode laser that was controlled by a home-built driver, producing 3 ns long pulses at a repetition rate of $f_{rep} = 48$ kHz. A quartz window at the top of the dip-stick allowed for optical access to image and localize areas of interest, and a microscope objective (NA = 0.8) was used to form an excitation spot measuring $\sim 1\ \mu m^2$. The power focused on this diffraction limited spot on top of the waveguide was measured outside the cryostat and the polarization orientation was controlled to be perpendicular to the antenna dipole axis in order to reduce the scattering of the pump laser. Time Correlated Single Photon Counting (TCSPC) electronics (Picoquant Picoharp 300) were used to record the PL decay traces, receiving the "start" event from the laser and "stop" event from the SNSPDs driver. Figure 3a displays a typical PL decay trace obtained after time-binning of the TCSPC data from QDs placed in an antenna gap. The response of the PbS/CdS QDs can clearly be separated from the residual pump laser pulse, however, there also is a considerable continuous wave (CW) background. Detector dark counts only contribute 150 cps to the background, the remainder has to originate either from the pump laser or the QDs. From the instrument response recorded on an empty antenna (see Supporting Information S6) we extracted that 80% of all laser counts should be CW and therefore assign the remainder of the background counts to the QDs. Using this reasoning, we estimate by integrating the counts in Figure 3a that for a typical count rate of 24 kcps recorded with the SNSPD, 8% are residual counts from the pump laser, 1% are dark counts, 25% are from the QD pulse and 66% are CW counts from the QDs. For varying pump power the extracted count rates for the pulsed and CW contribution of the QD emission are displayed in Figure 3c. While the CW part shows a linear increase with the excitation power, the pulsed contribution saturates as a result of fast Auger recombination suppressing any emission from multi-exciton states. Fitting the count rate from pulsed emission to the expected behavior for QDs emitting from a single-exciton state, yields an average number of excitations per QD in the antenna gap

$\langle n \rangle_{ant} = 0.84 \pm 0.07$, for a pump power of $P_{ant} = 800$ nW. This is in agreement with a value of $\langle n \rangle \sim 1.25$ estimated from the QD absorption cross-section and the photon flux at the pump wavelength in the Supporting Information S7, where losses induced by the objective lens focusing the laser on the sample were neglected. From the pulsed count rate of $c_{ant} = 6$ kcps

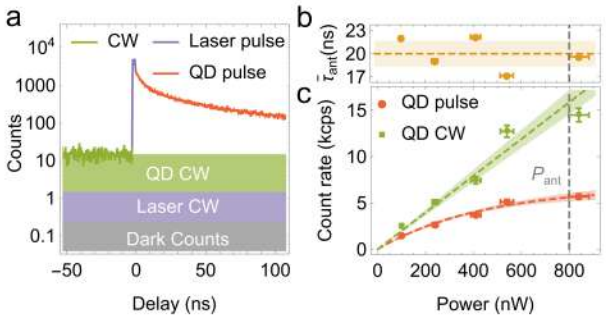

Figure 3: (a) PL decay trace recorded for QDs placed in the antenna gap using an excitation power of $P_{ant} = 800$ nW. (b) Excitation power dependence of the mean lifetime extracted from a stretched exponential fit. (c) Power dependence of the pulsed and CW contribution of the QD emission. The shaded areas show the 1-σ confidence intervals from the fit displayed as a dashed line.

it is possible to estimate the average quantum yield ϕ_{ant} of n_{QD} QDs in the antenna gap to be

$$\phi_{ant} = \frac{c_{ant}}{f_{rep}\, n_{QD}\, \langle n \rangle_{ant}\, \beta_{ant}\, \xi\, \eta_{ant}} \tag{2}$$

taking into account the waveguide coupling efficiency β_{ant}, the waveguide transmission ξ and the SNSPD detection efficiency η_{ant}.

From the size of the QD pillars and the packing density, we were able to estimate the number of excited QDs to be $n_{QD} = 200 \pm 50$ (see Supporting Information S5). Presuming that spherical PbS/CdS QDs show isotropic emission from their threefold degenerate bright exciton state[35] in a homogeneous environment, we argue that the high LRDOS in the antenna gap will force an emission polarization along the antenna dipole axis $\mathbf{d}$. FDTD simulations of the coupling to the transverse electric (TE) waveguide mode (see Supporting Information S8) predict a nearly constant coupling efficiency of $\beta_{ant} = 0.12$ within the volume of the QD pillar. For the waveguide transmission we measured $\xi = 0.9$ for the 1 cm long waveguide

connecting the antenna to the SNSPD, which has a detection efficiency of $\eta_{ant} = 0.9 \pm 0.1$ for the TE waveguide mode (see Supporting Information S2). Using these values we arrive at a quantum yield of $\phi_{ant} = 0.8 \pm 0.3\%$ for QDs in the antenna gap, which includes the metal losses from the antenna. We then used the same parameters to estimate the average number of excitations per QD due to the CW content of the pump laser and find an upper limit $\langle \mathrm{n} \rangle_{CW} < 0.01$ based on the observed CW count rate from the QDs under the assumption that an excitation lasts 1 μs on average. It can therefore be assured that the CW content of the laser does not unduly distort the extracted PL lifetimes.

In Figure 4d and e we compare the PL decay traces collected from an isolated pillar of QDs with QDs placed in the gap of an antenna on top of the same silicon nitride waveguide, assuring that a different detector behavior would not impede the results. The data was normalized and fitted with a stretched exponential

$$c(t) = a\ e^{-\left(\frac{t}{\tau_K}\right)^{\zeta}} \tag{3}$$

after subtraction of the background. This accounts for a distribution of decay times for $\zeta < 1$ and turns into an exponential decay expected for a single-exciton emission at $\zeta = 1$. To judge the effect of the plasmonic antennas on the QD PL lifetime, we then extracted the mean lifetime $\bar{\tau}$ from the fitted parameters according to

$$\bar{\tau} = \frac{\tau_K}{\zeta}\Gamma(\frac{1}{\zeta}), \tag{4}$$

using the gamma function Γ. Averaging the values for fourteen different QD pillars collected with different SNSPDs we obtained an expectation value for the mean lifetime from the QDs on a waveguide $\langle \bar{\tau}_0 \rangle = 138 \pm 27$ ns (Figure 4a) and $\langle \bar{\tau}_{ant} \rangle = 30 \pm 9$ ns for QDs in the antenna gaps (Figure 4b). To minimize the effect of unintended excitation through scattered laser light, individual antennas and isolated pillars were separated by 20 μm on the waveguides. Figure 3b shows further that the measured lifetime does not depend on the excitation power,

there is however a variation resulting from the fitting procedure.

FDTD simulations showed that for the chosen polarization direction of the laser perpendicular to the antenna dipole (see Supporting Information Figure S6), the excitation enhancement of the antennas is negligible. For isolated QD pillars the polarization control of the pump laser was removed, leading to an increased excitation power $P_0 \sim 2P_{ant}$, which results in an average excitation number per QD $\langle n \rangle_0 \sim 1$. Due to isotropic emission in absence of the antenna the coupling efficiency reduces to $\beta_0 = \frac{1}{3}(\beta_{TE} + \beta_{TM})$ with average values of $\beta_{TE} = \beta_{TM} = 0.11$ obtained from FDTD simulations (see Supporting Information S8). Since the isolated pillar of QDs equally couples to the TE and TM mode of the waveguide the SNSPD detection efficiency further reduces to $\eta_0 = \frac{1}{2}(\eta_{TE} + \eta_{TM}) = 0.8 \pm 0.1$. Comparing QDs in an antenna gap and isolated pillars on the same waveguide the change in quantum yield can be estimated as

$$\frac{\phi_{ant}}{\phi_0} = \frac{c_{ant}\,\langle n \rangle_0\,\beta_0\,\eta_0}{c_0\,\langle n \rangle_{ant}\,\beta_{ant}\,\eta_{ant}} \tag{5}$$

where c_0 is the pulsed count rate from an isolated QD pillar. The values reported in Figure 4c were corrected for the antenna absorption in case of multiple antennas on a single waveguide and correspond to the lifetimes at the same position in Figure 4b. For most antennas a short lifetime corresponds to a large enhancement of the quantum yield. Averaging over the reported data set we calculate $\langle \phi_{ant}/\phi_0 \rangle = 9.5 \pm 4.5$, the observed variation can be attributed to a misalignment of the QD pillar with respect to the antenna gap during the fabrication process. As a figure of merit for the antenna performance we finally calculate the radiative part of the local density of states

$$\mathrm{LRDOS} = \frac{\tau_0}{\tau_{ant}} \frac{\phi_{ant}}{\phi_0} \tag{6}$$

and obtain a mean value of $\langle \mathrm{LRDOS} \rangle = 44 \pm 26$ and a maximum of 200 ± 50, which is in good agreement with the results from FDTD simulations presented above.

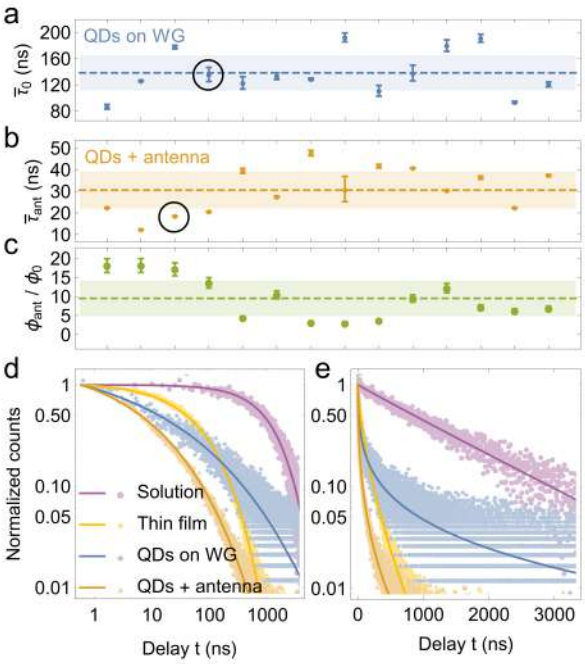

Figure 4: PL lifetime from different freestanding pillars of PbS/CdS QDs (a) and PbS/CdS QDs placed in the gap of plasmonic bowtie antennas (b) extracted from measurements with different SNSPDs. The quantum efficiency with an antenna ϕ_{ant} normalized to an isolated pillar ϕ_0 in (c) correspond to the lifetime measurements above. The dashed lines and shaded areas show the respective mean value and standard deviation, the displayed error bars are the 1-σ confidence intervals from the fit. The PL decay traces in (d) and (e) were normalized after subtraction of the background, the experimental data is overlaid with fitted stretched exponential functions. The circled data points in (a) and (b) were extracted from the respective decay traces in (d) and (e).

To understand the multi-exponential decay from pillars of PbS/CdS QDs at cryogenic temperatures we performed additional lifetime measurements of the same QD sample at room temperature in solution and for a 1 μm thick drop-cast film. The results are reported in Figure 4d and e and it can be clearly seen that for the sample in solution with a quantum yield of 8.5%, the decay is nearly single-exponential. The fitting procedure yields $\zeta = 0.97 \pm 0.02$ and a lifetime of $\overline{\tau}_{sol} = 1260 \pm 50$ ns, which is in line with PL lifetimes reported for similar QDs.[36] For the thin film at room temperature the lifetime drops to $\overline{\tau}_{TF} = 90 \pm 5$ ns accompanied by a reduction of the quantum yield to 2.5%. We hypothesize that is the result of a QD sample consisting of many dark dots and a subset of bright dots with a quantum yield

close to 100%. While in solution the dots are sufficiently separated to suppress interaction, in thin films energy transfer between adjacent QDs will lead to the observed multi-exponential decay by introducing additional non-radiative decay channels for dots which are bright in solution. The extensive processing of the QDs measured with the photonic chip at cryogenic temperatures might further reduce the fraction of bright dots, leading to an even lower average quantum yield of $\langle\phi_0\rangle = 0.05 \pm 0.03\%$ for isolated QD pillars on a waveguide.

The maximum LRDOS of 200 ± 50 measured on this integration platform shows its potential to reduce the lifetime of individual IR emitters. However, also the different count rate contributions are essential for targeting quantum applications. Based on the analysis above we estimate that using the antenna 91% of the total counts on the detector were from the QDs, 7% from residual pump laser transmission through the waveguide, 1% from differently scattered laser light, while 1% were dark counts. This suggests that the current corrugated sidewall grating filter with a pump suppression of 40 dB (see Supporting Information S10) should be further improved to reach the limit of what is possible on a single chip.[37] We also estimated a quantum yield of $\phi_{ant} = 0.8 \pm 0.3$ % for a pillar consisting of $n_{QD} = 200 \pm 50$ PbS/CdS QDs, accurately placed in the gap of a plasmonic antenna. Due to the low index contrast of the SiN waveguides and the SiO_2 cladding material, the coupling of the QD emission to the waveguide mode is only 12%, a value that could be readily increased by adding DBR mirrors, incorporating the QDs inside the waveguide[23] and partially removing the cladding material.[38] This means that by using brighter emitters and minor changes in the design, the integration platform presented here should allow to scale down to one emitter per antenna and thereby achieve single-photon emission. It can also be expected to obtain improved emission enhancement for ideally placed individual QDs. There has been some recent progress on single-photon emission from colloidal QDs emitting in the visible,[21,22] but improved emitters in the IR suitable for QKD with narrower linewidth and faster initial radiative decay have yet to become available.

On-chip lifetime spectroscopy

Wavelength Division Multiplexing (WDM) can increase the key generation rate for QKD and it is already widely used for conventional optical telecommunication. To multiplex and de-multiplex the signal from several sources to a single transmission channel and back to several detectors, Arrayed Waveguide Gratings (AWG) are the photonic component of choice. AWGs allow for a narrow channel spacing while keeping the device footprint small and have been successfully integrated with SNSPDs.[39] An alternative component is a Planar Concave Grating (PCG), which can perform better in terms of cross-talk between the channels, but typically has a larger footprint for a small channel spacing.[40] However, the ensemble PL spectrum of the PbS/CdS QDs we used for this work was very broad (see Figure 5b), so we opted for a PCG spectrometer to perform a wavelength-resolved on-chip PL lifetime characterization of the emitters instead. The spectrometer shown in Figure 5d was designed to have four channels connected to SNSPDs, which was the maximum number of detectors we were able to connect electrically in a single cool-down. The additional two channels of the PCG allowed for a passive characterization of the fabricated devices at room temperature prior to the measurements at cryogenic temperatures (see Supporting Information S9). Transmission measurements in Figure 5c show an insertion loss as low as 1.5 dB and a cross-talk below -20 dB for all channels, confirming the suitability of the silicon nitride passive photonic components for quantum applications.

To obtain enough signal for the wavelength resolved measurements, the number of QDs was increased by covering a 100 μm long section of the waveguide with multiple layers of QDs. Measuring with a single SNSPD connected to the waveguide, we observed a saturation of the extracted lifetime with respect to the excitation position shown in Figure 5f, indicating some influence of self-absorption on the measurement. For the preferred excitation position giving a maximum count rate on the detector, an average lifetime of $\bar{\tau} = 200 \pm 5$ ns was obtained. Using the spectrometer and four different SNSPDs the mean lifetime values in Figure 5a were extracted from the PL decay traces in Figure 5e and a clear increase of the

mean lifetime with increasing wavelength was observed. This observation is in contrast with the behavior in solution at room temperature,[36] but a very similar spectral dependence of the PL lifetime of PbS/CdS QD thin films has been observed at cryogenic temperatures.[41] Again, the correlation between longer emission wavelengths and longer lifetimes could reflect the influence of energy transfer on the emission of QDs in a close-packed thin film. To also collect a valid intensity spectrum of the QDs with the on-chip PCG, it would be necessary to calibrate for different detector efficiencies (see Supporting Information S2) prior to any measurements, which was not possible due to the limitations of the set-up.

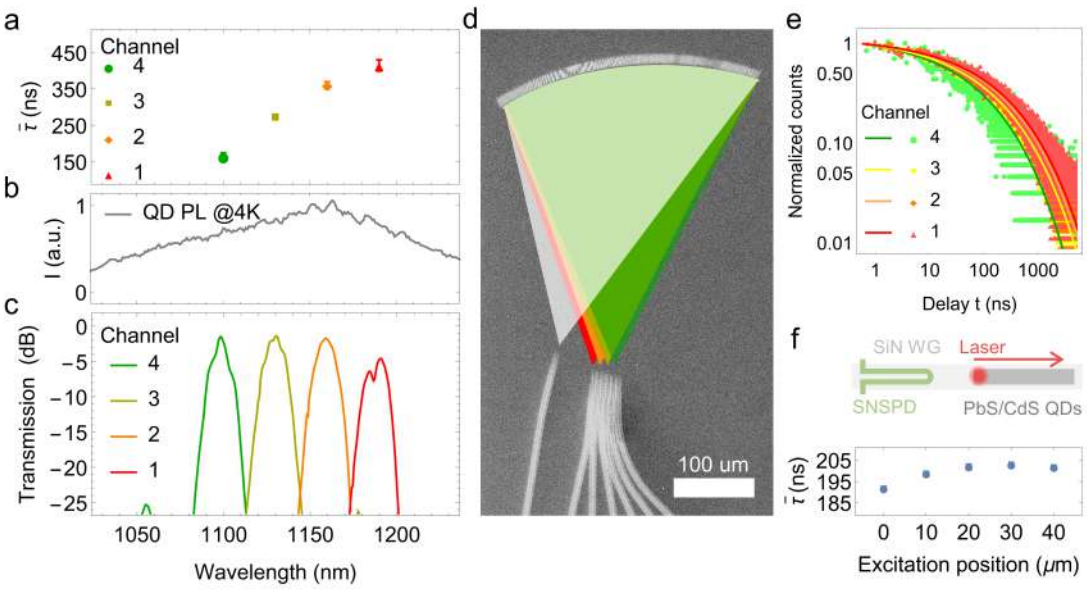

Figure 5: On-chip lifetime spectroscopy of PbS/CdS QDs. The lifetimes values in (a) were extracted using a stretched exponential fit of the PL decay traces measured with SNSPDs connected to the respective spectrometer channels. The emission spectrum of an embedded layer of PbS/CdS QD at 4.2K (b) matches the measured spectrometer channel transmissions in (c). The SEM micrograph in (d) shows the PCG spectrometer with a colored overlay visualizing the propagation of light from the input to the output arms. The PL decay traces in (f) were normalized after subtraction of the background, the experimental data is overlaid with fitted stretched exponential functions. The excitation position dependence of the lifetime in (f) was measured without the PCG using a single SNSPD.

In summary, we developed a method to reliably integrate and test several components required for QKD at cryogenic temperatures, showing their combined operation on-chip. These

are SNSPDs, plasmonic antennas to enhance the emission of IR-emitting colloidal PbS/CdS QDs and high-quality silicon nitride passive photonic components. Using these components we performed on-chip lifetime spectroscopy of PbS/CdS QDs at cryogenic temperatures and further demonstrated a maximum radiative local density of states (LRDOS) enhancement of 200 ± 50 for QDs deterministically placed in the antenna gap. The e-beam fabricated waveguides had a transmission loss below 1 dB/cm and the insertion loss of the spectrometer was 1.5 dB. The pump filter, achieving a suppression of -40 dB had an insertion loss below 1 dB. However, to realize a complete transceiver chip, further active photonic components are necessary to encode information either using path- or time-bin-encoding. Nanophotonic Pockels modulators[42] can achieve this functionality on a silicon nitride photonic platform. In addition, more suitable emitters than the colloidal PbS/CdS QDs in the current implementation, crucially with a higher ensemble PL quantum yield that would allow to work with individual single-photon emitters are necessary to be competitive with current on-chip implementations using attenuated lasers.[29] Importantly, the chip-based platform presented in this paper is flexible to changes and newly developed solution-processed emitters can be readily integrated.

Acknowledgement

This work was supported by the European Commission via the Marie-Sklodowska Curie action Phonsi (H2020-MSCA-ITN-642656). D.V.T. and Z.H. acknowledge the FWO-Vlaanderen for supporting this research (project nr. G087317N). R.G. thanks René Van Der Molen, Andréas Fognini and Johannes Los for technical support and beneficial discussions. I.E.Z. acknowledges the support of NWO LIFT-HTSM for Physics 2016-2017, project nr. 680-91-202 and support from Single Quantum B.V. (SQ).

Supporting Information Available

The supporting information contains details on chip design and fabrication, the waveguide-coupled SNSPDs, PbS/CdS QD synthesis and RT characterization, additional simulation and measurement data on the plasmonic bow-tie antennas, an estimation of the number of deposited QDs, the instrument response, details on the PCG used for the on-chip lifetime spectroscopy, the characterization of the pump filter and the original SEM micrographs used for the main part. This material is available free of charge via the Internet at http://pubs.acs.org.

References

(1) Aharonovich, I.; Englund, D.; Toth, M. Solid-state single-photon emitters. *Nat. Photonics* **2016**, *10*, 631–641.

(2) Burnham, D. C.; Weinberg, D. L. Observation of Simultaneity in Parametric Production of Optical Photon Pairs. *Phys. Rev. Lett.* **1970**, *25*, 84–87.

(3) Senellart, P.; Solomon, G.; White, A. High-performance semiconductor quantum-dot single-photon sources. *Nat. Nanotechnol.* **2017**, *12*, 1026–1039.

(4) Schwartz, I.; Cogan, D.; Schmidgall, E. R.; Don, Y.; Gantz, L.; Kenneth, O.; Lindner, N. H.; Gershoni, D. Deterministic generation of a cluster state of entangled photons. *Science* **2016**, *354*, 434–437.

(5) Loredo, J. C.; Broome, M. A.; Hilaire, P.; Gazzano, O.; Sagnes, I.; Lemaitre, A.; Almeida, M. P.; Senellart, P.; White, A. G. Boson Sampling with Single-Photon Fock States from a Bright Solid-State Source. *Phys. Rev. Lett.* **2017**, *118*, 130503.

(6) Reindl, M.; Huber, D.; Schimpf, C.; da Silva, S. F. C.; Rota, M. B.; Huang, H.;

Zwiller, V.; Jöns, K. D.; Rastelli, A.; Trotta, R. All-photonic quantum teleportation using on-demand solid-state quantum emitters. *Sci. Adv.* **2018**, *4*, eaau1255.

(7) Marsili, F.; Verma, V. B.; Stern, J. A.; Harrington, S.; Lita, A. E.; Gerrits, T.; Vayshenker, I.; Baek, B.; Shaw, M. D.; Mirin, R. P.; Nam, S. W. Detecting single infrared photons with 93% system efficiency. *Nat. Photonics* **2013**, *7*, 210–214.

(8) Schuck, C.; Pernice, W. H. P.; Tang, H. X. Waveguide integrated low noise NbTiN nanowire single-photon detectors with milli-Hz dark count rate. *Sci. Rep.* **2013**, *3*, 1893.

(9) Esmaeil Zadeh, I.; Los, J. W. N.; Gourgues, R. B. M.; Steinmetz, V.; Bulgarini, G.; Dobrovolskiy, S. M.; Zwiller, V.; Dorenbos, S. N. Single-photon detectors combining high efficiency, high detection rates, and ultra-high timing resolution. *APL Photonics* **2017**, *2*, 111301.

(10) Pernice, W.; Schuck, C.; Minaeva, O.; Li, M.; Goltsman, G.; Sergienko, A.; Tang, H. High-speed and high-efficiency travelling wave single-photon detectors embedded in nanophotonic circuits. *Nat. Commun.* **2012**, *3*, 1325.

(11) Schuck, C.; Pernice, W. H. P.; Tang, H. X. NbTiN superconducting nanowire detectors for visible and telecom wavelengths single photon counting on Si3N4 photonic circuits. *Appl. Phys. Lett.* **2013**, *102*, 051101.

(12) Reithmaier, G.; Lichtmannecker, S.; Reichert, T.; Hasch, P.; Müller, K.; Bichler, M.; Gross, R.; Finley, J. J. On-chip time resolved detection of quantum dot emission using integrated superconducting single photon detectors. *Sci. Rep.* **2013**, *3*, 1901.

(13) Rath, P.; Kahl, O.; Ferrari, S.; Sproll, F.; Lewes-Malandrakis, G.; Brink, D.; Ilin, K.; Siegel, M.; Nebel, C.; Pernice, W. Superconducting single-photon detectors integrated with diamond nanophotonic circuits. *Light Sci. Appl.* **2015**, *4*, e338–e338.

(14) Schwartz, M.; Schmidt, E.; Rengstl, U.; Hornung, F.; Hepp, S.; Portalupi, S. L.; Llin, K.; Jetter, M.; Siegel, M.; Michler, P. Fully On-Chip Single-Photon Hanbury-Brown and Twiss Experiment on a Monolithic Semiconductor-Superconductor Platform. *Nano Lett.* **2018**, *18*, 6892–6897.

(15) Zadeh, I. E.; Elshaari, A. W.; Jöns, K. D.; Fognini, A.; Dalacu, D.; Poole, P. J.; Reimer, M. E.; Zwiller, V. Deterministic Integration of Single Photon Sources in Silicon Based Photonic Circuits. *Nano Lett.* **2016**, *16*, 2289–2294.

(16) Kim, J.-H.; Aghaeimeibodi, S.; Richardson, C. J. K.; Leavitt, R. P.; Englund, D.; Waks, E. Hybrid Integration of Solid-State Quantum Emitters on a Silicon Photonic Chip. *Nano Lett.* **2017**, *17*, 7394–7400.

(17) Elshaari, A. W.; Zadeh, I. E.; Fognini, A.; Reimer, M. E.; Dalacu, D.; Poole, P. J.; Zwiller, V.; Jöns, K. D. On-chip single photon filtering and multiplexing in hybrid quantum photonic circuits. *Nat. Commun.* **2017**, *8*, 379.

(18) Davanco, M.; Liu, J.; Sapienza, L.; Zhang, C.-Z.; De Miranda Cardoso, J. V.; Verma, V.; Mirin, R.; Nam, S. W.; Liu, L.; Srinivasan, K. Heterogeneous integration for on-chip quantum photonic circuits with single quantum dot devices. *Nat. Commun.* **2017**, *8*, 889.

(19) Katsumi, R.; Ota, Y.; Kakuda, M.; Iwamoto, S.; Arakawa, Y. Transfer-printed single-photon sources coupled to wire waveguides. *Optica* **2018**, *5*, 691.

(20) Correa, R. E.; Dauler, E. A.; Nair, G.; Pan, S. H.; Rosenberg, D.; Kerman, A. J.; Molnar, R. J.; Hu, X.; Marsili, F.; Anant, V.; Berggren, K. K.; Bawendi, M. G. Single photon counting from individual nanocrystals in the infrared. *Nano Lett.* **2012**, *12*, 2953–2958.

(21) Chandrasekaran, V.; Tessier, M. D.; Dupont, D.; Geiregat, P.; Hens, Z.; Brainis, E.

Nearly Blinking-Free, High-Purity Single-Photon Emission by Colloidal InP/ZnSe Quantum Dots. *Nano Lett.* **2017**, *17*, 6104–6109.

(22) Park, Y.-S.; Lim, J.; Klimov, V. I. Asymmetrically strained quantum dots with non-fluctuating single-dot emission spectra and subthermal room-temperature linewidths. *Nature Materials* **2019**, *18*, 249–255.

(23) Xie, W.; Gomes, R.; Aubert, T.; Bisschop, S.; Zhu, Y.; Hens, Z.; Brainis, E.; Van Thourhout, D. Nanoscale and Single-Dot Patterning of Colloidal Quantum Dots. *Nano Lett.* **2015**, *15*, 7481–7487.

(24) Preskill, J.; Shor, P. W. Simple Proof of Security of the BB84 Quantum Key Distribution Protocol. *Phys. Rev. Lett.* **2000**, *85*, 441–444.

(25) Lo, H.-K.; Ma, X.; Chen, K. Decoy State Quantum Key Distribution. *Phys. Rev. Lett.* **2005**, *94*, 230504.

(26) Lo, H.-K.; Curty, M.; Tamaki, K. Secure quantum key distribution. *Nat. Photonics* **2014**, *8*, 595–604.

(27) Boaron, A.; Boso, G.; Rusca, D.; Vulliez, C.; Autebert, C.; Caloz, M.; Perrenoud, M.; Gras, G.; Bussières, F.; Li, M.-J.; Nolan, D.; Martin, A.; Zbinden, H. Secure Quantum Key Distribution over 421 km of Optical Fiber. *Phys. Rev. Lett.* **2018**, *121*, 190502.

(28) Takemoto, K.; Nambu, Y.; Miyazawa, T.; Sakuma, Y.; Yamamoto, T.; Yorozu, S.; Arakawa, Y. Quantum key distribution over 120 km using ultrahigh purity single-photon source and superconducting single-photon detectors. *Sci. Rep.* **2015**, *5*, 14383.

(29) Sibson, P.; Erven, C.; Godfrey, M.; Miki, S.; Yamashita, T.; Fujiwara, M.; Sasaki, M.; Terai, H.; Tanner, M. G.; Natarajan, C. M.; Hadfield, R. H.; O'Brien, J. L.; Thompson, M. G. Chip-based quantum key distribution. *Nat. Commun.* **2017**, *8*, 13984.

(30) Akselrod, G. M.; Weidman, M. C.; Li, Y.; Argyropoulos, C.; Tisdale, W. A.; Mikkelsen, M. H. Efficient Nanosecond Photoluminescence from Infrared PbS Quantum Dots Coupled to Plasmonic Nanoantennas. *ACS Photonics* **2016**, *3*, 1741–1746.

(31) Hoang, T. B.; Akselrod, G. M.; Mikkelsen, M. H. Ultrafast Room-Temperature Single Photon Emission from Quantum Dots Coupled to Plasmonic Nanocavities. *Nano Lett.* **2016**, *16*, 270–275.

(32) Koenderink, A. F. Single-Photon Nanoantennas. *ACS Photonics* **2017**, *4*, 710–722.

(33) Chen, Y.; Ryou, A.; Friedfeld, M. R.; Fryett, T.; Whitehead, J.; Cossairt, B. M.; Majumdar, A. Deterministic Positioning of Colloidal Quantum Dots on Silicon Nitride Nanobeam Cavities. *Nano Lett.* **2018**, *18*, 6404–6410.

(34) Kinkhabwala, A.; Yu, Z.; Fan, S.; Avlasevich, Y.; Müllen, K.; Moerner, W. E. Large single-molecule fluorescence enhancements produced by a bowtie nanoantenna. *Nat. Photonics* **2009**, *3*, 654–657.

(35) An, J. M.; Franceschetti, A.; Zunger, A. The Excitonic Exchange Splitting and Radiative Lifetime in PbSe Quantum Dots. *Nano Lett.* **2007**, *7*, 2129–2135.

(36) Justo, Y.; Geiregat, P.; Hoecke, K. V.; Vanhaecke, F.; De Mello Donega, C.; Hens, Z. Optical properties of PbS/CdS Core/shell quantum dots. *J. Phys. Chem. C* **2013**, *117*, 20171–20177.

(37) Piekarek, M.; Bonneau, D.; Miki, S.; Yamashita, T.; Fujiwara, M.; Sasaki, M.; Terai, H.; Tanner, M. G.; Natarajan, C. M.; Hadfield, R. H.; O'Brien, J. L.; Thompson, M. G. High-extinction ratio integrated photonic filters for silicon quantum photonics. *Opt. Lett.* **2017**, *42*, 815.

(38) Bisschop, S.; Guille, A.; Van Thourhout, D.; Hens, Z.; Brainis, E. Broadband enhance-

ment of single photon emission and polarization dependent coupling in silicon nitride waveguides. *Opt. Express* **2015**, *23*, 13713.

(39) Kahl, O.; Ferrari, S.; Kovalyuk, V.; Vetter, A.; Lewes-Malandrakis, G.; Nebel, C.; Korneev, A.; Goltsman, G.; Pernice, W. Spectrally multiplexed single-photon detection with hybrid superconducting nanophotonic circuits. *Optica* **2017**, *4*, 557.

(40) Rahim, A. et al. Expanding the Silicon Photonics Portfolio with Silicon Nitride Photonic Integrated Circuits. *J. Light. Technol.* **2017**, *35*, 639–649.

(41) Temperature-Dependent Optical Properties of PbS/CdS Core/Shell Quantum Dot Thin Films: Probing the Wave Function Delocalization. *J. Phys. Chem. C* **2015**, *119*, 17480–17486.

(42) Alexander, K.; George, J. P.; Verbist, J.; Neyts, K.; Kuyken, B.; Van Thourhout, D.; Beeckman, J. Nanophotonic Pockels modulators on a silicon nitride platform. *Nat. Commun.* **2018**, *9*, 3444.
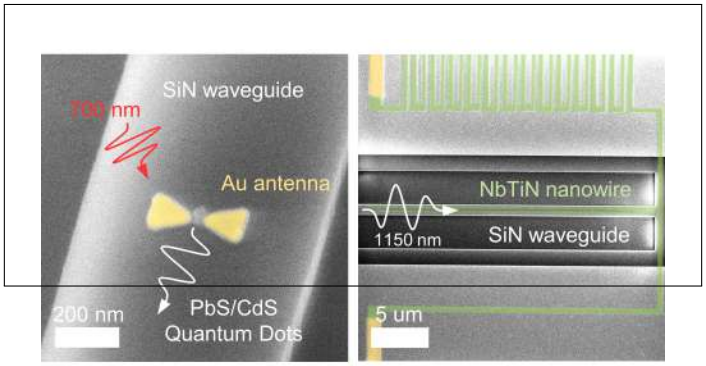
Graphical TOC Entry